# Channel-Mediated Tonic GABA Release from Glia

Soojung Lee, *et al.*

*Science* **330**, 790 (2010);
DOI: 10.1126/science.1184334

*This copy is for your personal, non-commercial use only.*

**If you wish to distribute this article to others**, you can order high-quality copies for your colleagues, clients, or customers by clicking here.

**Permission to republish or repurpose articles or portions of articles** can be obtained by following the guidelines here.

***The following resources related to this article are available online at www.sciencemag.org (this information is current as of November 4, 2010 ):***

**Updated information and services,** including high-resolution figures, can be found in the online version of this article at:
http://www.sciencemag.org/cgi/content/full/330/6005/790

**Supporting Online Material** can be found at:
http://www.sciencemag.org/cgi/content/full/science.1184334/DC1

This article **cites 46 articles**, 16 of which can be accessed for free:
http://www.sciencemag.org/cgi/content/full/330/6005/790#otherarticles

This article appears in the following **subject collections**:
Neuroscience
http://www.sciencemag.org/cgi/collection/neuroscience

*Science* (print ISSN 0036-8075; online ISSN 1095-9203) is published weekly, except the last week in December, by the American Association for the Advancement of Science, 1200 New York Avenue NW, Washington, DC 20005. Copyright 2010 by the American Association for the Advancement of Science; all rights reserved. The title *Science* is a registered trademark of AAAS.

# Channel-Mediated Tonic GABA Release from Glia

Soojung Lee,[1]* Bo-Eun Yoon,[1,2,5]* Ken Berglund,[3] Soo-Jin Oh,[1,2] Hyungju Park,[1] Hee-Sup Shin,[1,2] George J. Augustine,[2,3,4] C. Justin Lee[1,2,5]†

Synaptic inhibition is based on both tonic and phasic release of the inhibitory transmitter γ-aminobutyric acid (GABA). Although phasic GABA release arises from $Ca^{2+}$-dependent exocytosis from neurons, the mechanism of tonic GABA release is unclear. Here we report that tonic inhibition in the cerebellum is due to GABA being released from glial cells by permeation through the Bestrophin 1 (Best1) anion channel. We demonstrate that GABA directly permeates through Best1 to yield GABA release and that tonic inhibition is eliminated by silencing of Best1. Glial cells express both GABA and Best1, and selective expression of Best1 in glial cells, after preventing general expression of Best1, fully rescues tonic inhibition. Our results identify a molecular mechanism for tonic inhibition and establish a role for interactions between glia and neurons in mediating tonic inhibition.

A tonic form of synaptic inhibition that causes sustained activation of γ-aminobutyric acid (GABA) receptors in neurons (*1*) occurs throughout the central nervous system (*2*–*4*). Because of its sustained nature, tonic inhibition dominates over conventional (phasic) synaptic inhibition in controlling neuronal excitability (*1*). Therefore, tonic inhibition plays an important role in neuronal information processing (*5*) and has been implicated in epilepsy, sleep, memory, and cognition (*6*–*8*). The mechanism underlying the tonic release of GABA and the source of this GABA are poorly understood. We have addressed this question in cerebellar granule cells, which are powerfully restrained by tonic inhibition resulting from GABA released via an unconventional mechanism that is independent of action potentials and does not require vesicular exocytosis (*9*, *10*).

We hypothesized that tonic inhibition is mediated by GABA permeating through an anion channel, Best1 (*11*), previously implicated in glutamate release from astrocytes (*12*). Best1 has several features that make it attractive as a hypothetical mediator of tonic GABA release. Best1 is an anion channel that is activated by intracellular $Ca^{2+}$ and by changes in cell volume, though it is tonically active even at resting $Ca^{2+}$ levels and at normal cell volume. Best1 has unique permeability properties among anion channels, with a significant permeability to $HCO_3^-$ ($P_{HCO3}/P_{Cl} = 0.44$) (*13*) and a much higher permeability to large anions, such as $SCN^-$, than to $Cl^-$ (*14*). This channel is even permeable to gluconate ($P_{gluconate}/P_{Cl} = 0.4$) (*14*) and to the neurotransmitter, glutamate (*12*). Thus, Best1 might be permeable to GABA and thereby mediate tonic GABA release.

**Best1 is a GABA-permeable channel.** We first determined the permeability of Best1 to GABA (*15*). Best1 channels were expressed in human embryonic kidney–293 (HEK293T) cells, and whole-cell patch-clamp measurements were used to determine the reversal potential of the resulting ionic currents. Best1 channels were maximally activated by high (~4.5 μM) free $Ca^{2+}$ solution dialyzed into the cell upon establishment of the whole-cell configuration. The voltage dependence of currents flowing through Best1 was determined as illustrated in Fig. 1A (black trace). The reversal potential of the Best1-mediated current was +2.9 ± 4.4 mV ($n = 5$), which closely matched the equilibrium potential of +1 mV predicted for $Cl^-$. This indicates a current carried by $Cl^-$ under these conditions. This current was not observed in the presence of an anion channel blocker, 5-nitro-2-(3-phenylpropylamino)benzoic acid (NPPB), and was very small in the complete absence of internal $Ca^{2+}$ (Fig. 1, A and B). Two lines of evidence indicate that this current is caused by Best1. First, currents were absent in cells that were not transfected with Best1 (fig. S1). Second, making a tryptophan-to-cysteine residue mutation (W93C) in Best1 that is known to block the pore of the Best2 anion channel (*16*) eliminated all $Ca^{2+}$-activated current (Fig. 1, A and B). Thus, Best1 behaves as an anion channel, consistent with previous conclusions (*17*).

The GABA permeability of the Best1 channel was examined by replacing $Cl^-$ in the intracellular solution with GABA (Fig. 1C). The reversal potential of the current varied with intracellular GABA concentration (Fig. 1D). These shifts in reversal potential indicate that the GABA permeability of Best1 is substantial, although less than that of $Cl^-$. At an intracellular GABA concentration of 120 mM, the permeability of GABA relative to $Cl^-$ ($P_{GABA}/P_{Cl}$) was 0.27. Even though GABA is predominantly zwitterionic, the amount of GABA in anionic form is sufficient to carry considerable current, as indicated by current flow when GABA is the only permeant species (fig. S1).

Next, the $Ca^{2+}$ dependence of the GABA flux was examined by measuring current (at –80 mV) produced by various intracellular $Ca^{2+}$ concentrations (Fig. 1E). The half-maximal $Ca^{2+}$ concentration was calculated to be 150 nM with a Hill coefficient of 1.4 (Fig. 1F). Thus, GABA efflux is substantial even at basal cytosolic $Ca^{2+}$ levels of about 100 nM (*18*). The reversal potential of this current was identical at all intracellular $Ca^{2+}$ concentrations, which indicated that GABA permeability is unaffected by $Ca^{2+}$ (*18*).

To determine whether such GABA efflux through Best1 can be detected by a neighboring cell, we developed a two-cell biosensor microassay. GABA released through Best1 channels expressed in one HEK293T cell was detected via a second HEK293T cell that expressed GABA subtype C ($GABA_C$) receptors (Fig. 2A). Unlike the heteromeric $GABA_A$ receptors that mediate tonic inhibition in hippocampus and cerebellum (*19*), the $GABA_C$ receptor that mediates tonic inhibition in the retina (*20*) forms homomeric channels after expression of only a single subunit (*21*). $GABA_C$ receptors have a high affinity for GABA (*22*) and slow desensitization kinetics (*23*), which facilitate detection of tonic GABA release (*20*). The internal solution for cells expressing Best1 contained 3 or 140 mM GABA, and Best1 was activated by $Ca^{2+}$ concentrations of 100 nM or 4.5 μM.

We confirmed that Best1 displayed a significant permeability to GABA (Fig. 2B, top trace), indicated by an inward current flow at –80 mV, and that this current was associated with release of GABA onto the sensor cell (Fig. 2B, bottom trace). GABA release depended on permeation through Best1, because it was absent in conditions that block Best1, such as NPPB treatment and the W93C mutation (Fig. 2, C and D). To quantify the amount of GABA release, we normalized the response to the maximal current produced by bath application of 100 μM GABA (Fig. 2B, inset). With this approach we could compare GABA release under a variety of conditions (Fig. 2E) and reach a number of conclusions. First, GABA release was very small when Best1 was not expressed and could not be detected from cells expressing the W93C mutation. Second, GABA release was evident even at resting intracellular $Ca^{2+}$ concentration (100 nM) and could be detected when intracellular GABA concentration was as low as 3 mM. At high intracellular concentrations of $Ca^{2+}$ (4.5 μM) and GABA (140 mM), the amount of GABA released was so large that it nearly saturated (80% maximal) GABA receptors on the sensor cells. Third, GABA release was completely abolished by the anion channel blockers NPPB and niflumic acid (NFA); this was not due to a direct action of these com-

---

[1] Center for Neural Science, Korea Institute of Science and Technology (KIST), Seoul, Korea. [2] Center for Functional Connectomics, Korea Institute of Science and Technology (KIST), Seoul, Korea. [3] Department of Neurobiology, Duke University Medical Center, Durham, NC 27710, USA. [4] Program in Neuroscience and Behavioral Disorders, Duke-NUS Graduate Medical School, Singapore. [5] Neuroscience Program, University of Science and Technology (UST), Daejeon, Korea.

*These authors contributed equally to this work.

†To whom correspondence should be addressed. E-mail: cjl@kist.re.kr

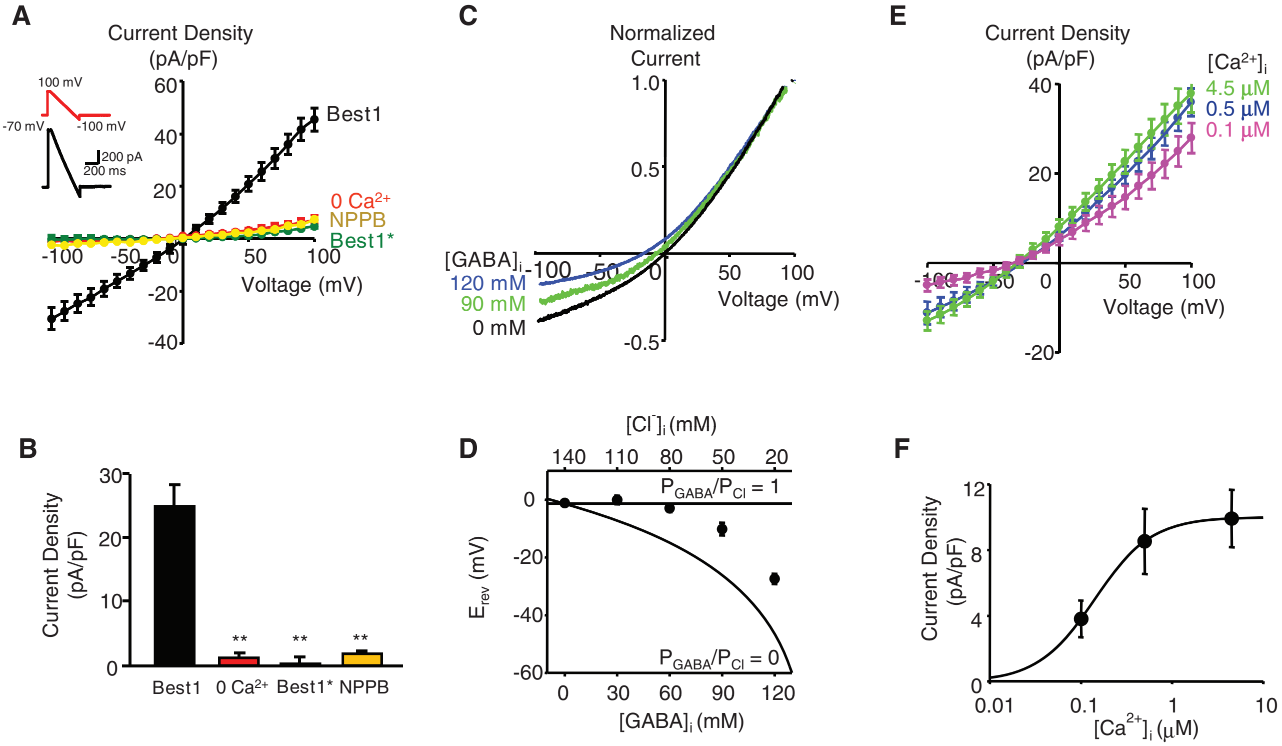

**Fig. 1.** Best1 is a GABA-permeable anion channel. (**A**) Relations between membrane potential (voltage) and mean current density measured in HEK293T cells expressing Best1 in the absence (0 $Ca^{2+}$, $n = 5$) and presence of $Ca^{2+}$ (~4.5 µM, $n = 5$). Current density was greatly reduced by expressing Best1 with a channel pore mutation, Best1-W93C (Best1*, $n = 5$), or by treatment with the anion channel blocker NPPB (100 µM, $n = 6$). Inset shows the protocol used to measure the relations between current (black) and voltage (red); in all cases intracellular $Cl^-$ concentration was 154 mM. (**B**) Summary of mean current density measured at –80 mV for each condition in (A). Throughout this research article, numerical values indicate means ± SEM unless otherwise indicated. Asterisks above bars indicate a significant difference determined by unpaired two-tailed *t* test ($P < 0.01$). (**C**) Voltage dependence of Best1 current in HEK293T cells (~4.5 µM intracellular $Ca^{2+}$) at the indicated intracellular GABA concentrations. In all cases, GABA was substituted for $Cl^-$, and each current trace was normalized to the current measured at +100 mV. (**D**) Dependence of current reversal potential ($E_{rev}$) on intracellular GABA concentration ($n = 7$ to 14 for each point). Continuous curves are $E_{rev}$ predicted by the Goldman-Hodgkin-Katz equation when GABA is as permeable as $Cl^-$ ($P_{GABA}/P_{Cl} = 1$) and when GABA is not permeable at all ($P_{GABA}/P_{Cl} = 0$). (**E**) Relations between membrane potential and mean current density measured in HEK293T cells at the indicated intracellular $Ca^{2+}$ concentrations ($n = 5$ to 7). Intracellular solution also contained 140 mM GABA. (**F**) Mean current densities recorded at –80 mV at different intracellular $Ca^{2+}$ concentrations. Continuous curve indicates a fit of the Hill equation with an $EC_{50}$ of 150 nM and a Hill coefficient of 1.4.

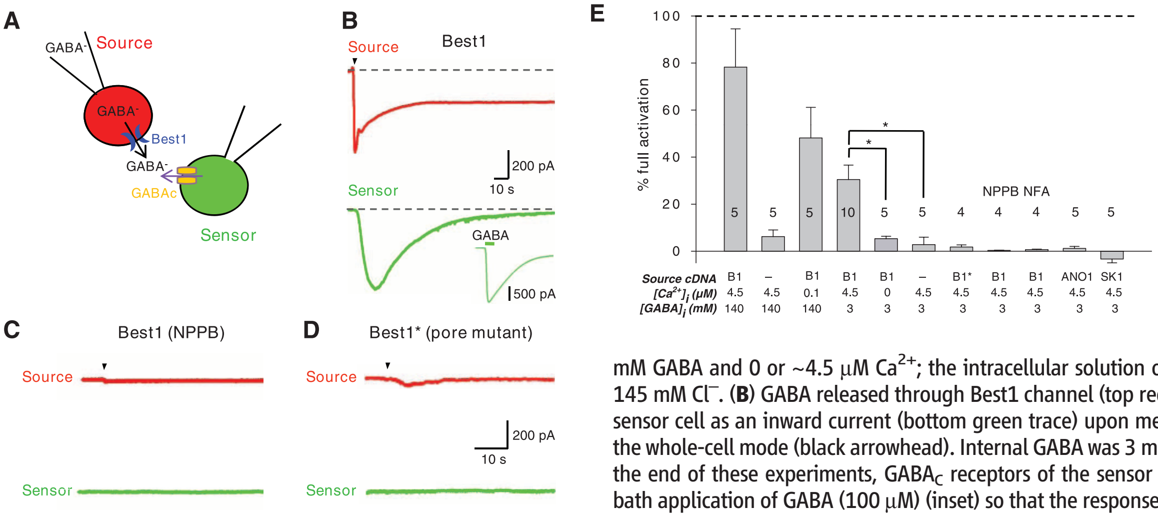

**Fig. 2.** GABA release via permeation through Best1 channels. (**A**) Schematic of two-cell bioassay. One HEK293T cell (Source) expressed Best1 and was labeled with dsRed; a second HEK cell (Sensor) expressed $GABA_C$ receptors and was labeled with GFP. The intracellular solution for the source cell contained 3 or 140 mM GABA and 0 or ~4.5 µM $Ca^{2+}$; the intracellular solution of the sensor cell contained 145 mM $Cl^-$. (**B**) GABA released through Best1 channel (top red trace) was detected in the sensor cell as an inward current (bottom green trace) upon membrane breakthrough into the whole-cell mode (black arrowhead). Internal GABA was 3 mM, and $Ca^{2+}$ was 4.5 µM. At the end of these experiments, $GABA_C$ receptors of the sensor cell were fully activated by bath application of GABA (100 µM) (inset) so that the response to released GABA could be normalized according to the number of GABA receptors expressed in the sensor cell. Time-dependent reductions in sensor cell currents are due to desensitization of GABA receptors. (**C**) GABA release was blocked by NPPB (100 µM). (**D**) No GABA release was observed when the source cell expressed the pore mutant Best1-W93C. (**E**) GABA release measured in the indicated conditions, with values normalized as described above. NPPB and NFA were applied at 100 µM. SK1 is small conductance $Ca^{2+}$-activated $K^+$ channel. ANO1 is a recently characterized $Ca^{2+}$-activated chloride channel. Numbers indicate the number of replicates in each condition, and asterisk indicates a significant difference ($P < 0.05$).

pounds on $GABA_C$ receptors (fig. S10, a and b). Finally, GABA release could not be reconstituted by expression of other $Ca^{2+}$-activated channels, such as the anion channel Ano1 (or TMEM-16A) or the potassium channel SK1 (Fig. 2E, and fig. S2) (*24*).

**Best1 mediates tonic GABA release in cerebellum.** We next asked whether treatments that interfere with Best1 function reduce tonic inhibition of cerebellar granule cells. We first used whole-cell patch-clamp recordings to measure the sustained $Cl^-$ current associated with tonic inhibition (*9*) (Fig. 3A). Treatment of granule cells with the $GABA_A$ receptor antagonist, GABAzine (SR95531 or SR; 10 μM), shifted this current by 35.7 ± 4.1 pA ($n = 8$), presumably by blocking $GABA_A$ receptors activated by tonic GABA release (*9*). Treatment with NPPB also reduced the tonic current by 19.0 ± 2.5 pA ($n = 8$). This blockade of tonic GABA current by NPPB was not due to a direct action of this compound on granule cell $GABA_A$ receptors (fig. S10, c and d). Two other anion channel blockers that block Best1, NFA and 4,4′-diisothiocyanatostilbene-2,2′-disulfonic acid disodium salt hydrate (DIDS), similarly reduced tonic inhibitory currents in granule cells (fig. S11, b and g). The degree of inhibition by these anion channel blockers ranged from about 50 to 75% of the total GABAzine-sensitive current.

To more selectively inhibit Best1 function, we constructed a lentivirus carrying a small hairpin–forming interference RNA (shRNA) targeted against Best1 (*12*). This virus also contained DNA encoding a fluorescent marker, mCherry, that permitted visualization of the location and amount of viral infection. When Best1-shRNA lentivirus was injected into the cerebellar cortex of these mice, infected cells (red) were distributed widely in the molecular layer, as well as in the granule cell layer (Fig. 3B, top left). Quantification of Best1 immunoreactivity (Fig. 3C) indicated that regions expressing Best1-shRNA had significantly decreased ($P < 0.003$; $n = 3$) Best1 levels in comparison with nearby uninfected regions (Fig. 3B, top right), whereas there was no such difference in mice injected with the control scrambled-shRNA (Fig. 3B, bottom right, and 3C).

To examine the effects of Best1 deletion (knockdown) on tonic inhibition, cerebellar slices were prepared from mice injected with either Best1-shRNA or scrambled-shRNA viruses, or from uninjected (naïve) mice. The ability of NPPB to block tonic current was eliminated in granule cells from mice injected with Best1-shRNA and was present at control levels (naïve) in granule cells from mice injected with scrambled-shRNA (Fig. 3D). Likewise, the total GABAzine-sensitive tonic current was significantly decreased in granule cells from mice injected with Best1-shRNA lentivirus, relative to cells from naïve mice or mice injected with scrambled-shRNA virus (Fig. 3E). Total GABAzine-sensitive tonic current was reduced by ~75% by Best1 knockdown (Fig. 3E), consistent with the results obtained with channel-blocking drugs. The source of the remaining tonic inhibition requires further investigation.

We next visualized the spatial extent of tonic inhibition by using the optogenetic indicator, Clomeleon (*25*), to image $Cl^-$ fluxes associated with tonic inhibition of granule cells (*26*). Cerebellar slices from a transgenic mouse line that expresses Clomeleon in cerebellar granule cells (Fig. 3F) were treated with 10 μM GABAzine to block tonic inhibition. This treatment markedly decreased intracellular $Cl^-$ concentration ($[Cl^-]_i$) in both granule cell bodies and their axons, parallel fibers. NPPB also lowered $[Cl^-]_i$, although the yellow color of this drug prevented accurate determination of $[Cl^-]_i$. To evaluate the role of Best1 in this $Cl^-$ influx, we compared the GABAzine-induced changes in $[Cl^-]_i$ in slices from Clomeleon mice

**Fig. 3.** Tonic GABA current was reduced by attenuation of Best1. (**A**) Representative measurement of tonic current in a cerebellar granule cell held at –60 mV during treatment with NPPB (50 μM, yellow bar) and then GABAzine (SR, 10 μM, blue bar). Arrows indicate magnitude of tonic current blocked by each drug. (**B**) Fluorescence images of the granule cell layer (GCL) and the molecular layer (ML) in a histological section from a cerebellum injected with lentiviruses transducing either Best1-shRNA (top) or scrambled RNA (bottom). The viruses also transduced the fluorescent protein mCherry (left), to indicate infected cells. shRNA treatment reduced Best1 immunoreactivity (right) in the Best1-shRNA infected area but not in the area infected with scrambled shRNA. (**C**) Efficiency of Best1 knockdown by scrambled shRNA (Scram) and Best1 shRNA (B1-shRNA). Immunoreactivity was normalized to fluorescence values measured in uninfected regions. (**D**) Magnitude of NPPB-sensitive tonic current recorded in granule cells treated as indicated. (**E**) Magnitude of SR-sensitive tonic current recorded in the same conditions. (**F**) Clomeleon fluorescence in cerebellar slice from CLM1 transgenic mouse. $[Cl^-]_i$ was measured in granule cell layer (GCL, red) and parallel fibers (PF, green). (**G**) Time course of $[Cl^-]_i$ changes reported by Clomeleon during SR application in GCL (red) and PF (green). Clomeleon transgenic mice were injected with either scrambled shRNA (top traces) or Best1-shRNA (bottom traces). (**H**) SR-sensitive changes in $[Cl^-]_i$ measured in the indicated conditions. Asterisks indicate a significant difference determined by unpaired two-tailed *t* test ($*P < 0.05$, $**P < 0.01$, $***P < 0.001$), while ns indicates a nonsignificant difference ($P > 0.05$).

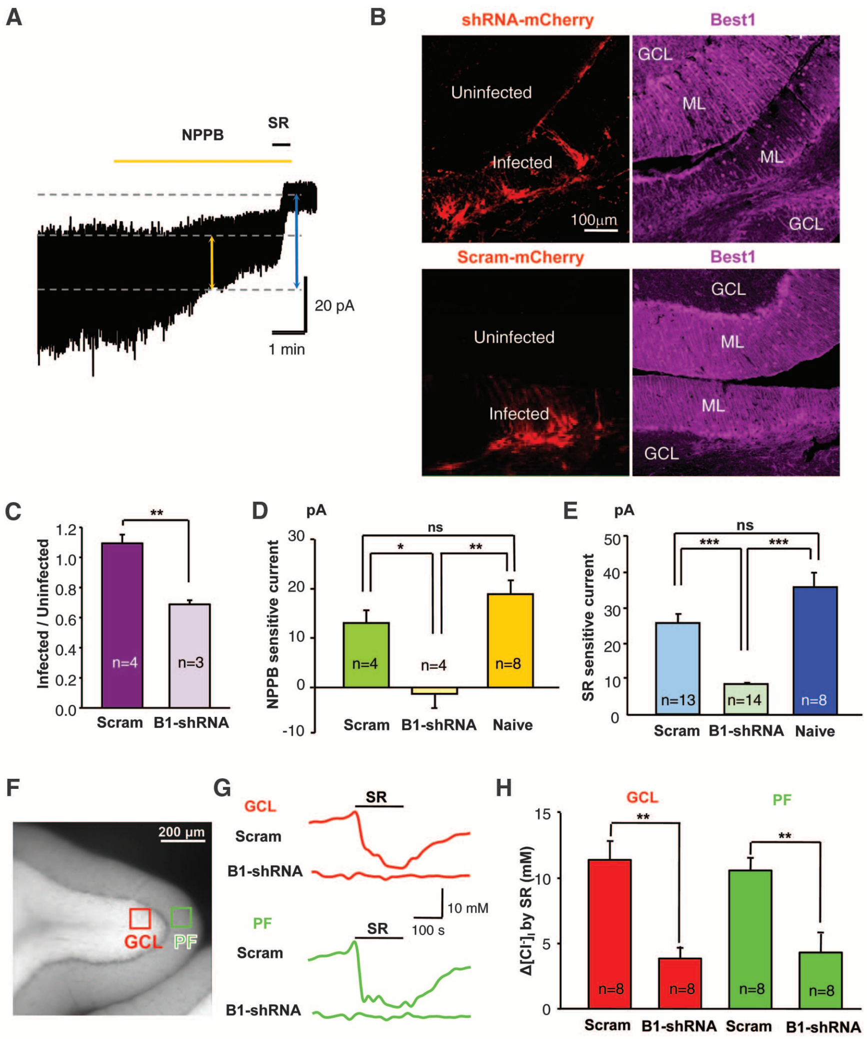

in which either the Best1-shRNA or the scrambled-shRNA viruses were injected. For both granule cell bodies and parallel fibers, the $[Cl^-]_i$ changes produced by GABAzine were significantly decreased in slices from mice injected with Best1-shRNA in comparison with mice injected with scrambled shRNA (Fig. 3G). On average, Best1-shRNA treatment reduced SR-sensitive tonic inhibition by 60% or more (Fig. 3H), consistent with our electrophysiological results.

**Glial cells contain GABA and express Best1 channel.** Having identified a molecular mediator of tonic GABA release, we next used this information to identify the cellular source of the GABA release. We used immunohistochemical labeling to identify cells within the cerebellum that contain both Best1 and GABA (Fig. 4, A and B, and fig. S4). The specificity of the Best1 antibody was confirmed by Western blot analysis (fig. S3) (*12*). Best1 and GABA immunoreactivity colocalized in GABA-mediated Purkinje cells (asterisks) and interneurons (white arrowheads), but not in glutamatergic granule cells (Fig. 4C). Remarkably, both Best1 and GABA apparently were highly expressed in Bergmann glial cells (arrows), a point we examined further using GFAP-GFP transgenic mice, which have green fluorescent protein (GFP)–labeled astrocytes (Fig. 4D) (*27*). In these mice, GFP-positive Bergmann glial cells contained both Best1 (Fig. 4E) and GABA (Fig. 4F), even in Bergmann glial processes (Fig. 4, E and F, and fig. S4b) that closely interact with parallel fibers (*28*). In addition, both GABA and Best1 were expressed in lamellar astrocytes adjacent to granule cell bodies (pale blue arrowheads in Fig. 4, E and F, and fig. S4a).

We thus reexamined the effects of Best1-shRNA treatment to determine which cells were affected by silencing of the Best1 gene (Fig. 4, G to I). To distinguish between neurons and glial cells, we again used GFAP-GFP transgenic mice and analyzed Best1 expression in cells that were GFP-positive (glia) or GFP-negative (neurons). Knockdown of Best1 was significant in glial cells (Fig. 4J) but not in neurons (Fig. 4K). This suggests that the U6 promoter drove shRNA expression more efficiently in glial cells than neurons, as reported for another promoter (*29*). There was no knockdown of Best1 in glia of mice injected with control, scrambled-shRNA (Fig. 4L).

Whole-cell patch-clamp recordings were used to determine whether Bergmann glial cells express functional, GABA-permeable Best1 channels. The internal solution contained either $Cl^-$ or GABA as the predominant anions, plus 4.5 μM free $Ca^{2+}$ to maximally activate Best1 channels. A Best1 blocker, NPPB (50 μM), reduced a tonic

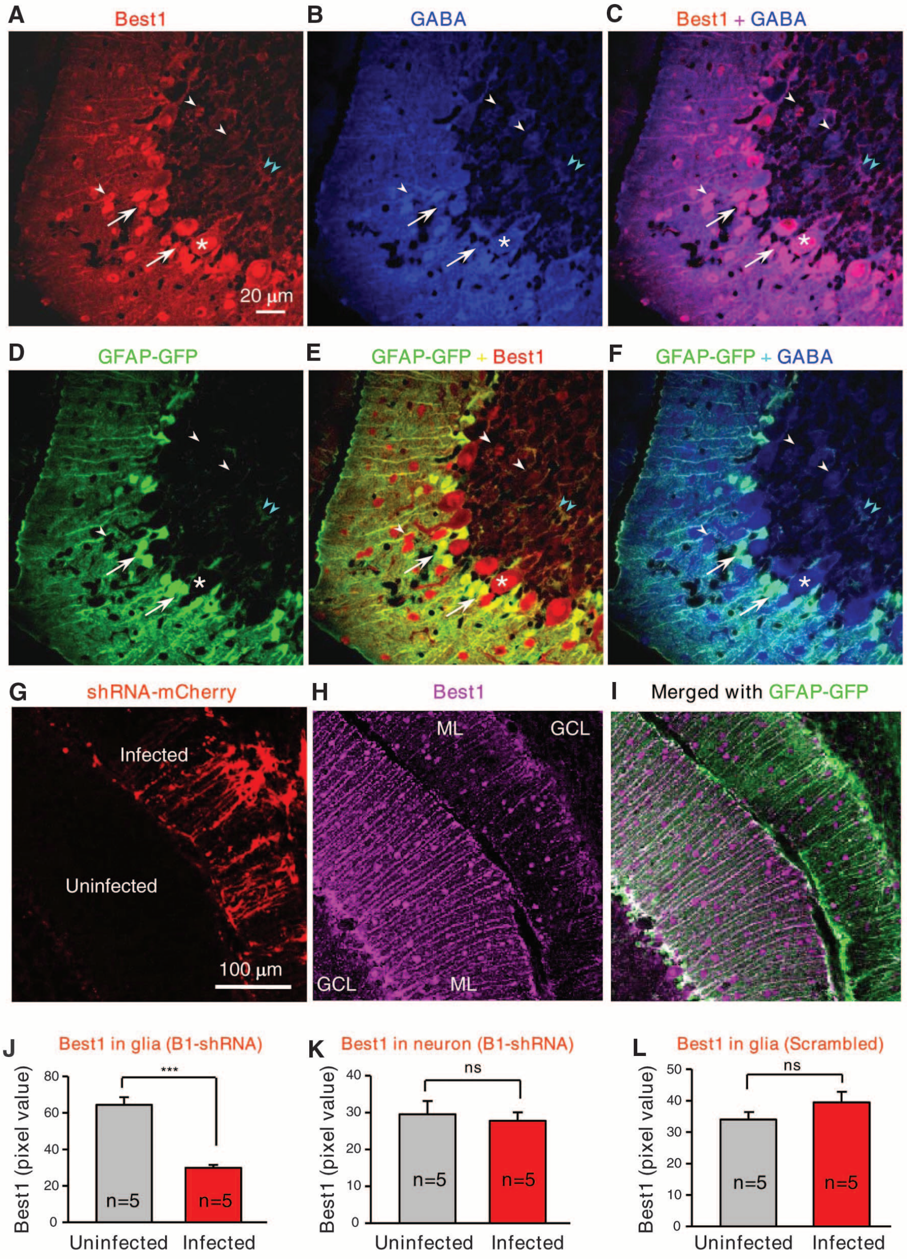

**Fig. 4.** Presence of both GABA and Best1 in cerebellar glial cells. (**A** to **F**) Immunostaining for Best1 (A), GABA (B), and GFP (D) in sections from GFAP-GFP transgenic mice. The indicated image pairs are superimposed in (C), (E), and (F). Best1 and GABA were coexpressed in Purkinje cells (asterisk), interneurons (white arrowheads), Bergmann glia (arrows), and lamellar astrocytes (pale blue arrowheads), but not in granule cells. All GFP-positive astrocytes robustly expressed Best1 (E) and evinced GABA staining (F). (**G** to **I**) Images from the cerebellum of a GFAP-GFP mouse injected with Best1-shRNA lentivirus carrying mCherry (G). Best1 labeling (H) was merged with GFAP-GFP (I) (**J** to **L**) Quantification of Best1 expression in glia [GFP-positive pixels (J)]; in neurons [GFP-negative pixels (K)]; in infected and uninfected regions of cerebellar tissue from mice injected with Best1-shRNA, as well as in glia injected with scrambled-shRNA (L). Asterisks indicate a significant difference determined by unpaired two-tailed *t* test (***$P < 0.001$); ns indicates a nonsignificant difference ($P > 0.05$).

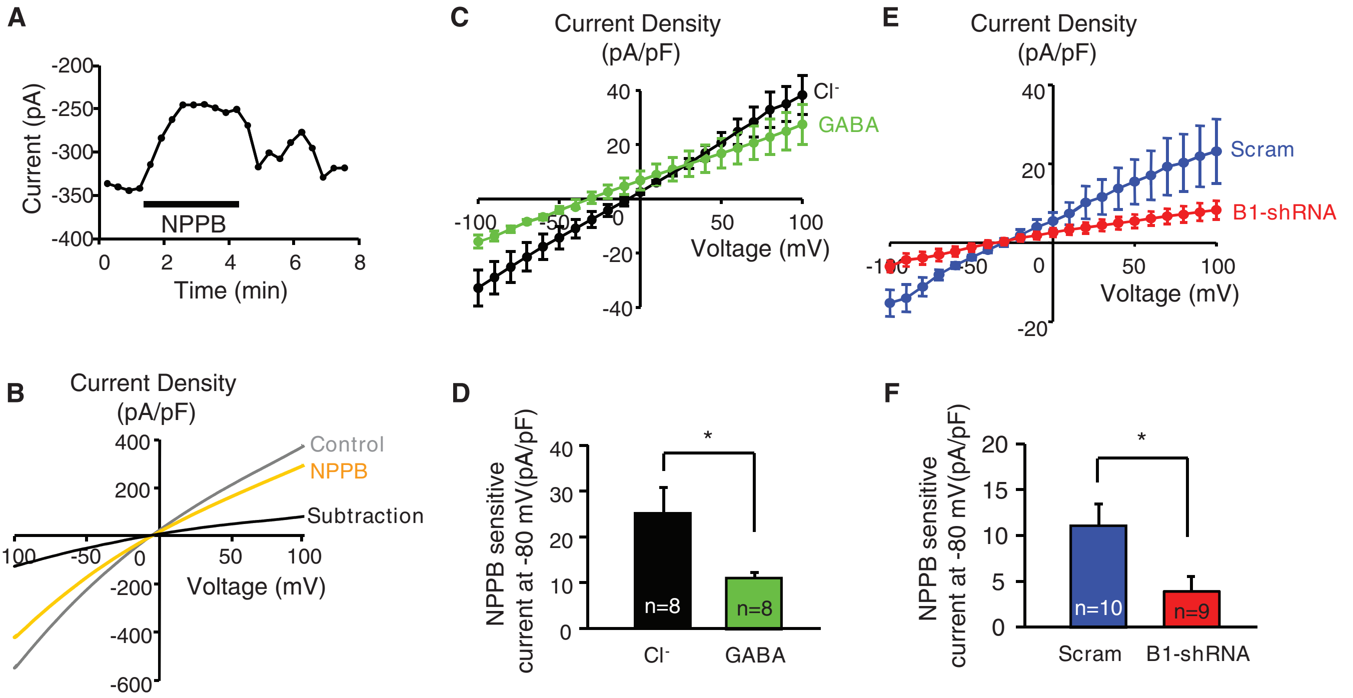

**Fig. 5.** Bergmann glia express GABA-permeable Best1 channels. (**A**) Current measured at –70 mV from a GFP-positive Bergmann glial cell in a cerebellar slice from a naïve GFAP-GFP mouse. Intracellular solution contained ~4.5 μM $Ca^{2+}$ and 150 mM $Cl^-$, as well as $Cs^-$ (146 mM) to block $Ca^{2+}$-dependent $K^+$ channels. Current was decreased by application of the anion channel blocker, NPPB (50 μM, bar). (**B**) Voltage dependence of currents, determined as in Fig. 1, measured before and during NPPB application. The difference between these two relations (subtraction) represents NPPB-sensitive current. (**C**) Voltage dependence of NPPB-sensitive current measured when internal solution contained $Cl^-$ (150 mM) or GABA (140 mM). (**D**) Mean amplitude of NPPB-sensitive currents measured at –80 mV with either $Cl^-$ or GABA inside the Bergmann glial cells. (**E**) Voltage dependence of NPPB-sensitive current measured in Bergmann glia from cerebella injected with scrambled shRNA (Scram) or Best1-shRNA (B1-shRNA). Internal solution contained 140 mM GABA. (**F**) Mean amplitude of NPPB-sensitive currents measured at –80 mV for the two conditions shown in (E). Asterisk indicates a significant difference determined by unpaired two-tailed *t* test ($P < 0.05$).

**Fig. 6.** Glia-specific rescue of Best1 restores tonic inhibition. (**A**) Viral transduction in cerebellum of tamoxifen-injected hGFAP-CreERT2 mice. (Left) Expression of mCherry, indicating virus-infected regions. (Middle) Best1 immunoreactivity in regions infected or uninfected by lentivirus. (Right) Merged images of mCherry, Best1, and GFP immunoreactivity. Note that, in this figure, the mCherry signal was electronically enhanced, relative to the images shown in other figures, because mCherry expression was reduced by tamoxifen treatment. (**B** and **C**) Quantification of Best1 immunoreactivity in hGFAP-CreERT2 mice injected with control solution (sunflower oil: – Tamoxifen) (B) or with tamoxifen (C). Asterisk indicates a significant difference ($P < 0.05$). (**D**) Tonic inhibition of granule cells measured in cerebellar slices from hGFAP-CreERT2 mice treated with tamoxifen and shRNA (shRNA +) or control mice (treated with sunflower oil: shRNA –) and compared with naïve, uninjected mice. Magnitude of tonic inhibition was determined from mean amplitude of current change produced by GABAzine application. (**E**) Magnitude of NPPB-sensitive current measured in the indicated conditions. (**F**) Model for tonic inhibition in the cerebellum: GABA is tonically released from glial cells via Best1 and activates GABA receptors on cell bodies and axons (parallel fibers) of granule cells. Asterisks indicate a significant difference determined by unpaired two-tailed *t* test (*$P < 0.05$, *** $P < 0.001$); ns indicates a nonsignificant difference ($P > 0.05$).

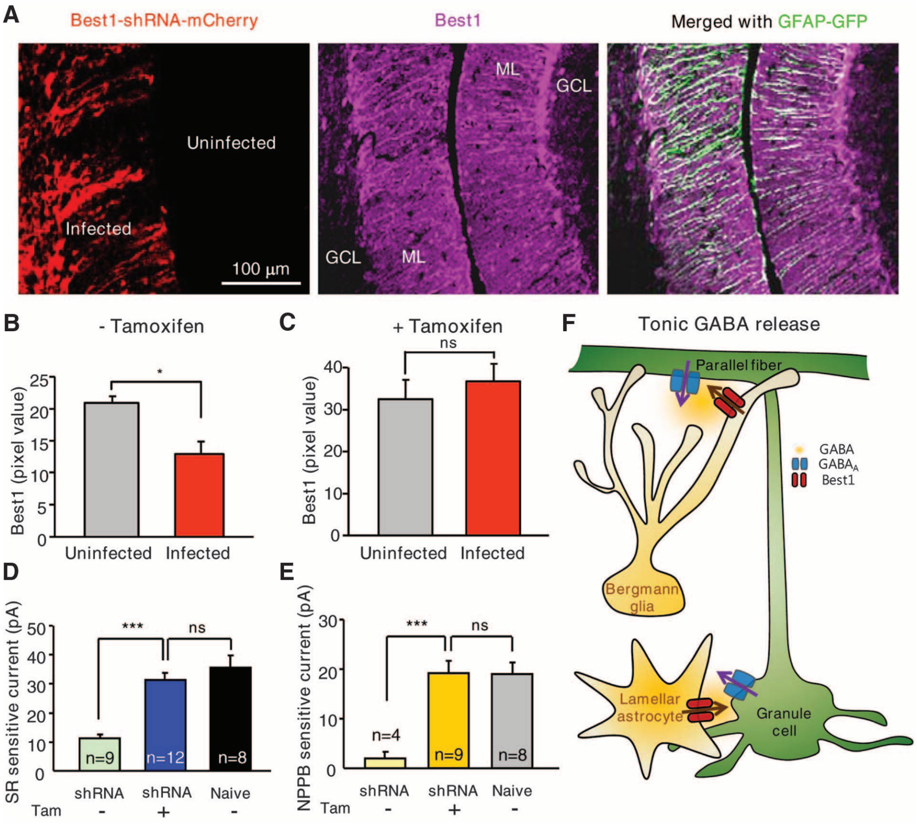

current in these cells (Fig. 5A). The voltage dependence of this current was determined by subtracting currents recorded during NPPB application from those measured before NPPB application (Fig. 5B). The NPPB-sensitive current measured with $Cl^-$ as the predominant internal anion showed a reversal potential of –3.4 mV (Fig. 5C), which was similar to the reversal potential of +1 mV predicted for a $Cl^-$ current and similar to Best1-expressing HEK293T cells (Fig. 1A). When GABA was the main internal anion (140 mM), the NPPB-sensitive current was inward at –80 mV, which indicated a significant efflux of GABA at this potential (Fig. 5, C and D). By measuring the reversal potential, we determined that the NPPB-sensitive anion current had a $P_{GABA}/P_{Cl}$ of 0.19 (Fig. 5C), similar to Best1-expressing HEK293T cells (Fig. 1D).

We further tested the function of Best1 in Bergmann glia by examining the effect of Best1-shRNA treatment on these cells (fig. S8). Compared with scrambled-shRNA, treatment with Best1-shRNA decreased the NPPB-sensitive conductance (the slope of the current-voltage relations) in Bergmann glia without changing the reversal potential (Fig. 5E and fig. S8, c and d). The effect on NPPB-sensitive GABA efflux was quantified by measuring current magnitude at –80 mV: GABA efflux at this potential was significantly smaller in Bergmann glia from mice injected with Best1-shRNA than with scrambled-shRNA (Fig. 5F, red) or from naïve mice (Fig. 5D, green).

**Glial Best1 is responsible for tonic GABA release.** To determine whether tonic GABA release is due to glial Best1, we used a molecular genetic strategy (*30*): Best1-shRNA was used to suppress Best1 expression throughout the cerebellar cortex, while selectively sparing Best1 expression in glia (*30*) (fig. S5). In hGFAP-CreERT2 mice treated with Best1-shRNA, glial Best1 (Fig. 6, A and B) and GABAzine-sensitive tonic current (Fig. 6D and fig. S9d) were significantly reduced, similar to those of wild-type mice (Fig. 3, C and E, and fig. S9a). However, treating the hGFAP-CreERT2 mice with tamoxifen before Best1-shRNA injection reduced mCherry expression (fig. S7), fully restored Best1 immunoreactivity (Fig. 6, A and C), and fully ($P < 0.001$) rescued GABAzine-sensitive currents to levels observed in naïve animals (Fig. 6D and fig. S9). Similarly, NPPB-sensitive tonic currents were reduced by shRNA and fully rescued in tamoxifen-treated mice (Fig. 6E).

**Discussion.** We found that tonic release of the major inhibitory transmitter, GABA, is due to direct permeation of GABA through the anion channel, Best1, and that this release originates predominantly from glial cells. The mechanism underlying tonic GABA release has been difficult to elucidate because tonic GABA release exhibits several puzzling features that are quite different from those exhibited by conventional, phasic release of GABA. Our proposed mechanism can account for each of these properties: (i) the nonvesicular nature of tonic GABA release is consistent with a channel-mediated mechanism; (ii) the independence from neuronal activity can be explained by the glial origins of tonic inhibition; and (iii) the apparent lack of dependence on external $Ca^{2+}$ arises from substantial activation of Best1 at resting levels of intracellular $Ca^{2+}$ (Fig. 1F), which leads to constitutive release of GABA at such intracellular $Ca^{2+}$ levels (Fig. 2) (*17*, *31*).

Our results provide several independent lines of evidence indicating that GABA is permeable through Best1. These include (i) shifts in current reversal potential when intracellular GABA concentration was varied (Fig. 1, C and D); (ii) current flow when GABA is the only permeant ion (fig. S1); and (iii) Best1-dependent release of GABA from one cell onto another (Fig. 2). Collectively, these results demonstrate that GABA permeates through Best1. Although it has been proposed that Best1 has functions in addition to being an ion channel (*17*, *32*, *33*), our finding that a channel pore mutation blocks GABA release (Fig. 2D) indicates that GABA is released by direct permeation through the Best1 channel pore. We presume that tonic inhibition is caused by GABA (*34*); it remains a formal possibility that it is mediated by some other molecule that permeates Best1 and activates GABA receptors, such as taurine (fig. S12).

To cause efflux through the Best1 channel, intracellular GABA concentration in Bergmann glial cells should be high enough to maintain the required electrochemical gradient. Bergmann glial cells show GABA immunoreactivity as intense as that observed in neighboring inhibitory neurons (Fig. 4B), which suggests a high GABA content, consistent with the intracellular GABA concentration of 3.5 mM reported in cultured astrocytes (*35*). With a submicromolar extracellular concentration of GABA (*36*), such high intracellular concentrations yield a positive equilibrium potential for GABA. Given the very negative resting-membrane potential of Bergmann glial cells, there is a strong electrochemical gradient to drive GABA efflux through the Best1 channel.

The GABA sensitivity [median effective concentration ($EC_{50}$) = 1.1 μM, Hill coefficient = 2.1] of $GABA_C$ receptors (*22*) used in our two-cell biosensor microassay can be used to estimate a peak extracellular GABA concentration of 500 nM with 4.5 μM $Ca^{2+}$ and 3 mM intracellular GABA concentration (Fig. 1E). At resting $Ca^{2+}$ (100 nM), GABA efflux through Best1 is 31% of that measured at 4.5 μM $Ca^{2+}$ (Fig. 1, E and F); this would yield an extracellular GABA concentration of 155 nM, which is remarkably close to the extracellular GABA concentration of 160 nM thought to be present during tonic inhibition (*36*).

Our work is consistent with previous indications that glia release GABA (*37*–*39*). Because Best1 is also volume-sensitive, our results provide a mechanism for the observation that swelling can trigger GABA release from glia (*37*). GABA usually is thought to be synthesized, contained, and released exclusively by neurons in adult brain. However, a handful of reports have suggested that astrocytes contain GABA (*40*), and our immunohistochemical data provide further support for this idea. Although our work does not identify the source of GABA in Bergmann glia, it is known that GABA can be synthesized in glia via two pathways (*41*) and can be taken up into glia by GABA transporters (*42*).

The spatial organization of cerebellar glial cells is ideally suited to provide ambient GABA for tonic inhibition. In the type II glomerulus, the sheaths of lamellar astrocytes (*43*) are intimately associated with granule cell dendrites (*44*, *45*). Such structures could permit the tonic inhibition of granule cell bodies and dendrites (*9*). Likewise, Bergmann glial cells tightly wrap around parallel fiber synapses (*46*, *47*), providing a strategic location for tonic inhibition of parallel fibers (*46*). Our findings lead to a model for tonic GABA release (Fig. 6F): GABA in Bergmann glia permeates through the Best1 channel to activate $GABA_A$ receptors on parallel fibers, while the same mechanisms allow lamellar astrocytes to tonically inhibit granule cell bodies and dendrites. By providing a source of GABA and by locating the molecular machinery for tonic GABA release near the granule cell structures, as well as by creating a restricted volume that allows tonic accumulation of GABA, it appears that glial cells are anatomically optimized for controlling electrical signaling in neighboring cerebellar neurons.

In conclusion, we have demonstrated an unprecedented mechanism for tonic GABA release through the bestrophin channel in cerebellar glial cells and propose a function for glia in modulating neuronal signaling via tonic inhibition.

### References and Notes

1. M. Farrant, Z. Nusser, *Nat. Rev. Neurosci.* **6**, 215 (2005).
2. T. S. Otis, K. J. Staley, I. Mody, *Brain Res.* **545**, 142 (1991).
3. M. Kaneda, M. Farrant, S. G. Cull-Candy, *J. Physiol.* **485**, 419 (1995).
4. S. G. Brickley, S. G. Cull-Candy, M. Farrant, *J. Physiol.* **497**, 753 (1996).
5. P. Chadderton, T. W. Margrie, M. Häusser, *Nature* **428**, 856 (2004).
6. D. W. Cope *et al.*, *Nat. Med.* **15**, 1392 (2009).
7. F. Jia *et al.*, *J. Neurophysiol.* **94**, 4491 (2005).
8. V. B. Caraiscos *et al.*, *Proc. Natl. Acad. Sci. U.S.A.* **101**, 3662 (2004).
9. D. J. Rossi, M. Hamann, D. Attwell, *J. Physiol.* **548**, 97 (2003).
10. M. J. Wall, M. M. Usowicz, *Eur. J. Neurosci.* **9**, 533 (1997).
11. K. Petrukhin *et al.*, *Nat. Genet.* **19**, 241 (1998).
12. H. Park *et al.*, *J. Neurosci.* **29**, 13063 (2009).
13. Z. Qu, H. C. Hartzell, *Am. J. Physiol. Cell Physiol.* **294**, C1371 (2008).
14. K. E. O'Driscoll, N. Leblanc, W. J. Hatton, F. C. Britton, *Biochem. Biophys. Res. Commun.* **384**, 476 (2009).
15. Materials and methods are available as supporting material on *Science* Online.
16. Z. Qu, L. T. Chien, Y. Cui, H. C. Hartzell, *J. Neurosci.* **26**, 5411 (2006).
17. H. C. Hartzell, Z. Qu, K. Yu, Q. Xiao, L. T. Chien, *Physiol. Rev.* **88**, 639 (2008).
18. D. E. Clapham, *Cell* **131**, 1047 (2007).
19. J. Glykys, I. Mody, *Neuron* **56**, 763 (2007).
20. S. M. Jones, M. J. Palmer, *J. Neurophysiol.* **102**, 691 (2009).
21. M. Chebib, *Clin. Exp. Pharmacol. Physiol.* **31**, 800 (2004).
22. J. E. Carland *et al.*, *Neuropharmacology* **46**, 770 (2004).
23. J. Amin, D. S. Weiss, *Receptors Channels* **2**, 227 (1994).
24. C. T. Bond, J. Maylie, J. P. Adelman, *Curr. Opin. Neurobiol.* **15**, 305 (2005).
25. T. Kuner, G. J. Augustine, *Neuron* **27**, 447 (2000).
26. K. Berglund *et al.*, *Brain Cell Biol.* **36**, 101 (2008).
27. M. Brenner, W. C. Kisseberth, Y. Su, F. Besnard, A. Messing, *J. Neurosci.* **14**, 1030 (1994).

28. T. Müller, H. Kettenmann, *Int. Rev. Neurobiol.* **38**, 341 (1995).
29. K. Takayama, T. Torashima, H. Horiuchi, H. Hirai, *Neurosci. Lett.* **443**, 7 (2008).
30. A. Ventura *et al.*, *Proc. Natl. Acad. Sci. U.S.A.* **101**, 10380 (2004).
31. S. Kirischuk, T. Möller, N. Voitenko, H. Kettenmann, A. Verkhratsky, *J. Neurosci.* **15**, 7861 (1995).
32. K. Yu, Z. Qu, Y. Cui, H. C. Hartzell, *Invest. Ophthalmol. Vis. Sci.* **48**, 4694 (2007).
33. K. Kunzelmann *et al.*, *Cell Calcium* **46**, 233 (2009).
34. P. Cavelier, M. Hamann, D. Rossi, P. Mobbs, D. Attwell, *Prog. Biophys. Mol. Biol.* **87**, 3 (2005).
35. J. Bardakdjian, M. Tardy, C. Pimoule, P. Gonnard, *Neurochem. Res.* **4**, 517 (1979).
36. V. Santhakumar, H. J. Hanchar, M. Wallner, R. W. Olsen, T. S. Otis, *J. Neurosci.* **26**, 3357 (2006).
37. A. S. Kozlov, M. C. Angulo, E. Audinat, S. Charpak, *Proc. Natl. Acad. Sci. U.S.A.* **103**, 10058 (2006).
38. S. Ochi *et al.*, *Glia* **9**, 188 (1993).
39. S. Oláh *et al.*, *Nature* **461**, 1278 (2009).
40. A. Blomqvist, J. Broman, *J. Neurocytol.* **17**, 629 (1988).
41. R. Martínez-Rodríguez *et al.*, *Cell Mol. Biol. (Noisy-le-grand)* **39**, 115 (1993).
42. A. Gadea, A. M. López-Colomé, *J. Neurosci. Res.* **63**, 461 (2001).
43. C. E. Ribak, W. M. Tong, N. C. Brecha, *Anat. Embryol. (Berlin)* **194**, 379 (1996).
44. V. Chan-Palay, S. L. Palay, *Z. Anat. Entwicklungsgesch.* **138**, 1 (1972).
45. D. M. Landis, L. A. Weinstein, J. J. Halperin, *Brain Res.* **284**, 231 (1983).
46. J. Grosche *et al.*, *Nat. Neurosci.* **2**, 139 (1999).
47. T. C. Bellamy, *Cerebellum* **5**, 116 (2006).
48. We thank J. Park for the ANO1 clone, J. Adelman for the human SK1 clone, K. Kunzelmann for mouse Best1 antibody, and J. Lee for image analysis. We specially thank K. McCarthy for his generous gift of hGFAP-CreERT2 transgenic mice. This study was supported by the KIST Core Competency Program and International Cooperation Program, by a Korean national honor scientist grant, an NIMH grant, and a World Class Institute grant to the Center for Functional Connectomics.

**Supporting Online Material**
www.sciencemag.org/cgi/content/full/science.1184334/DC1
Materials and Methods
SOM Text
Figs. S1 to S12
References

6 November 2009; accepted 3 September 2010
Published online 23 September 2010;
10.1126/science.1184334
Include this information when citing this paper.

---

# Collaborative Non-Self Recognition System in S-RNase–Based Self-Incompatibility

Ken-ichi Kubo,[1]* Tetsuyuki Entani,[1]* Akie Takara,[1] Ning Wang,[2] Allison M. Fields,[3] Zhihua Hua,[2]† Mamiko Toyoda,[1] Shin-ichi Kawashima,[1] Toshio Ando,[4] Akira Isogai,[1] Teh-hui Kao,[2,3]‡ Seiji Takayama[1]‡

**Self-incompatibility in flowering plants prevents inbreeding and promotes outcrossing to generate genetic diversity. In Solanaceae, a multiallelic gene, *S-locus F-box* (*SLF*), was previously shown to encode the pollen determinant in self-incompatibility. It was postulated that an SLF allelic product specifically detoxifies its non-self S-ribonucleases (S-RNases), allelic products of the pistil determinant, inside pollen tubes via the ubiquitin–26*S*-proteasome system, thereby allowing compatible pollinations. However, it remained puzzling how SLF, with much lower allelic sequence diversity than S-RNase, might have the capacity to recognize a large repertoire of non-self S-RNases. We used in vivo functional assays and protein interaction assays to show that in *Petunia*, at least three types of divergent SLF proteins function as the pollen determinant, each recognizing a subset of non-self S-RNases. Our findings reveal a collaborative non-self recognition system in plants.**

Self-incompatibility (SI) is an intraspecific reproductive barrier adopted by angiosperms that allows the pistil to distinguish between self (genetically related) and non-self (genetically unrelated) pollen. In most cases, this self/non-self discrimination is controlled by male- and female-specificity determinants (pollen-S, style-S) encoded by multiallelic genes at the *S* locus (*1*, *2*). Self-incompatible species in Solanaceae, Rosaceae, and Plantaginaceae use extracellular S-RNase as style-S (*3*). If the *S* haplotype of pollen matches either *S* haplotype of the style, S-RNase exerts cytotoxicity inside the self-pollen tube to inhibit growth (*3*). Pollen-S was identified as an F-box protein, named *S*-locus F-box (SLF or SFB) (*4*–*6*), which may be a component of an SCF (Skp1–Cullin1–F-box) or SCF-like complex (*7*, *8*).

A protein degradation model was proposed to explain *S* haplotype–specific rejection of pollen tubes by S-RNase. It predicts that an SLF allelic variant specifically recognizes its non-self S-RNases and mediates their degradation by the ubiquitin–26*S*-proteasome system (*1*, *8*, *9*). This model can explain competitive interaction, where SI breaks down in heteroallelic pollen carrying two different pollen-*S* alleles (*10*, *11*). Each SLF allelic product in heteroallelic pollen mediates degradation of all S-RNases except its self S-RNase, and two different SLF allelic products together mediate the degradation of all S-RNases, rendering the pollen tube compatible with styles of any *S* genotype (*3*, *8*). Experiments designed on the basis of competitive interaction showed that *PiSLF*$_2$ ($S_2$ allele of *Petunia inflata SLF*) functions as pollen-*S* (*6*). When *PiSLF*$_2$ was introduced into $S_1S_2$ and $S_2S_3$ plants, it caused breakdown of SI in $S_1$ and $S_3$ pollen, but not in $S_2$ pollen, as predicted by competitive interaction (*6*).

Thus far, *PiSLF*$_2$ is the only *SLF* allele in *Petunia* shown to function as pollen-*S* (*6*, *9*). *SLF* shows much lower allelic sequence diversity than *S-RNase*, and nonsynonymous substitution rates of *SLF*s from *Antirrhinum*, *Petunia*, and *Prunus* are 0.01 to 0.11, whereas those for *S-RNase* are 0.14 to 0.51 (*12*, *13*). Given the large number of *S* haplotypes within each species, it is puzzling how an SLF allelic product could recognize a large repertoire of highly divergent non-self S-RNases to allow cross-compatible pollinations. Moreover, phylogenetic studies of *SLF* and *S-RNase* in Solanaceae and Plantaginaceae showed no evidence of coevolution, with *SLF* having a much shorter evolutionary history (*12*), which is unexpected for the "male" and "female" genes encoding proteins directly involved in self/non-self discrimination during sexual reproduction. Here, we address the question of whether the previously identified SLF in *Petunia* is the only protein that constitutes the pollen determinant in SI.

**Previously studied *SLF* is not the sole element of pollen-*S*.** We first cloned four additional alleles of *Petunia SLF* from pollen cDNA of $S_5$, $S_7$, $S_9$, and $S_{11}$ homozygotes by 3′- and 5′-RACE (rapid amplification of cDNA ends) with the use of primers (table S1) designed on the basis of *PiSLF*$_1$, *PiSLF*$_2$, and *PiSLF*$_3$ sequences (*6*, *14*). The deduced amino acid sequences of all nine of the identified *SLF* alleles exhibited higher sequence similarities (86.4 to 100% identity) than the corresponding nine *S-RNase* alleles (40.1 to 79.4% identity) (fig. S1). Because the taxa with S-RNase–based SI have multiple *SLF*-like genes (*5*, *9*), we renamed *SLF* "type-1 *SLF*," designating alleles as $S_n$-*SLF1*, with *n* denoting the *S* haplotype.

A surprising finding from the sequence comparison was that the deduced amino acid sequence of $S_7$-*SLF1* is identical with that of $S_{19}$-*SLF1* (previously named *PaSLF*$_{19}$) (*11*), although the amino acid sequences of $S_7$- and $S_{19}$-RNase are 45% identical (fig. S1). Reciprocal pollinations between $S_7$ and $S_{19}$ homozygotes showed that all pollinations were compatible (Fig. 1A), confirming that $S_7$ and $S_{19}$ are distinct *S* haplotypes. The finding of the identical SLF1 in two different *S* haplotypes raised the possibility that SLF1 is not the sole element of pollen-S.

To address this possibility, we first examined whether $S_5$-, $S_7$- (= $S_{19}$-), $S_9$-, and $S_{11}$-*SLF1* function as pollen-*S*. We introduced each transgene construct (fig. S2) into appropriate *S* heterozygotes of *Petunia* (table S2) (*14*) and confirmed expression of each transgene in pollen by reverse transcription polymerase chain reaction (RT-PCR)

---

[1] Graduate School of Biological Sciences, Nara Institute of Science and Technology, 8916-5 Takayama, Ikoma 630-0192, Japan. [2] Intercollege Graduate Degree Program in Plant Biology, Pennsylvania State University, University Park, PA 16802, USA. [3] Department of Biochemistry and Molecular Biology, Pennsylvania State University, University Park, PA 16802, USA. [4] Graduate School of Horticulture, Chiba University, 648 Matsudo, Chiba 271-8510, Japan.

*These authors contributed equally to this work.

†Present address: Department of Genetics, University of Wisconsin, Madison, WI 53706, USA.

‡To whom correspondence should be addressed. E-mail: txk3@psu.edu (T.-h.K.); takayama@bs.naist.jp (S.T.)